

Reframing Music-Driven 2D Dance Pose Generation as Multi-Channel Image Generation

Yan Zhang Han Zou Lincong Feng Cong Xie Ruiqi Yu Zhenpeng Zhan
Global Business Unit, Baidu Inc.

Abstract

Recent pose-to-video models can translate 2D pose sequences into photorealistic, identity-preserving dance videos, so the key challenge is to generate temporally coherent, rhythm-aligned 2D poses from music, especially under complex, high-variance in-the-wild distributions. We address this by reframing music-to-dance generation as a music-token-conditioned multi-channel image synthesis problem: 2D pose sequences are encoded as one-hot images, compressed by a pretrained image VAE, and modeled with a DiT-style backbone, allowing us to inherit architectural and training advances from modern text-to-image models and better capture high-variance 2D pose distributions. On top of this formulation, we introduce (i) a time-shared temporal indexing scheme that explicitly synchronizes music tokens and pose latents over time and (ii) a reference-pose conditioning strategy that preserves subject-specific body proportions and on-screen scale while enabling long-horizon segment-and-stitch generation. Experiments on a large in-the-wild 2D dance corpus and the calibrated AIST++2D benchmark show consistent improvements over representative music-to-dance methods in pose- and video-space metrics and human preference, and ablations validate the contributions of the representation, temporal indexing, and reference conditioning. See supplementary videos in <https://hot-dance.github.io>

1. Introduction

Music-driven dance generation aims to synthesize human motions that are temporally coherent and synchronized with musical rhythm. In practical applications, the end goal is to produce a full video of a given person dancing on a given music track. Recent pose-to-video methods [5, 11] can already translate a 2D pose sequence into photorealistic, identity-preserving videos with strong fidelity. This work therefore focuses on the first stage—generating a sequence of 2D poses from music—which is the key bottleneck for controllable, rhythm-aligned dance video synthesis.

A large body of prior work [12, 13, 15–17, 22, 26, 29, 34, 38] targets music-to-3D motion generation. Although 3D motion can be projected to 2D pose keypoints, progress is constrained by the scarcity of synchronized music–motion pairs: capturing high-quality 3D dance typically requires multi-view rigs or motion-capture systems, which limits both scale and stylistic diversity. As a result, generalization across musical genres and styles remains challenging (see Table 2). In contrast, 2D in-the-wild dance videos are abundant and span broader musical genres and tempi, a wider range of body proportions (e.g., shoulder width, limb lengths), and richer dance styles (e.g., variations in tempo, expressiveness, or movement dynamics). This makes 2D a practical training route for building scalable and expressive music-conditioned generators.

However, training directly on in-the-wild 2D poses is challenging. Unlike canonical 3D motion benchmarks, the 2D data exhibit substantial variability in physical body proportions and in on-screen scale (how large the person appears in the frame). These factors increase the difficulty of jointly modeling dance motion, body proportion, and on-screen scale within a single generator. Our experiments further show that simply adapting methods originally designed for 3D motion to 2D data yields suboptimal results. Recent works, such as [4], attempt to train an autoregressive predictor on in-the-wild 2D data using raw 2D coordinates. In our experiments, we observe that raw coordinates are a suboptimal representation for dance pose generation in a diffusion-based setting.

To model the challenging in-the-wild 2D pose distribution, we recast music-to-pose generation as a *music-token-conditioned multi-channel image generation* problem. Concretely, we convert raw 2D coordinates into one-hot encodings and stack frames over time, yielding an image-like tensor where each channel exhibits smooth, curve-like trajectories along the temporal axis (Figure 1). The music waveform is mapped to a sequence of tokens by a pretrained music encoder. This reformulation allows us to directly leverage the modern toolchain of DiT-style text-token-conditioned image generation [7, 25, 27], which has demonstrated strong capacity to model complex, high-

variance distributions.

Our one-hot design is inspired by common practices in 2D pose detection, where one-hot encodings often outperform raw coordinate regression [18]. Analogous to standard pose detection, which infers keypoints from an image, our pose generator ‘detects’ poses from (music tokens + diffusion noise). We extend this intuition to generative modeling and validate its effectiveness through targeted ablations experiments.

Building on this reformulation, we introduce two mechanisms that further support practical deployment: (i) a position-indices alignment module that encourages beat-synchronous generation by aligning motion events with musical structure, and (ii) a reference-pose strategy that maintains long-range consistency of body proportions and local pose style across extended sequences.

In summary, our contributions are threefold: (1) we reframe music-to-dance generation as a music-token-conditioned multi-channel image synthesis problem with one-hot pose representation, thereby leveraging advances in modern text-to-image models; (2) we propose a time-shared temporal indexing scheme that explicitly synchronizes music tokens and pose latents over time, together with a reference-pose conditioning strategy that preserves subject-specific body proportions and on-screen scale while enabling long-horizon segment-and-stitch generation; and (3) we conduct extensive experiments on a large in-the-wild 2D dance corpus and the calibrated AIST++2D benchmark, showing that our model performs favorably against representative methods in pose- and video-space metrics and human preference.

2. Related Work

Music-to-dance generation. Most prior work synthesizes 3D motion from music [12, 13, 15–17, 22, 26, 29, 34, 38]. Building on cross-modal interaction, [15] introduces a cross-modal transformer to enhance motion quality via multimodal attention. [29] explores reinforcement learning to better align movement beats with musical beats. With the advent of denoising diffusion probabilistic models [10], [34] proposes a diffusion-based dance generator that denoises multiple overlapping motion segments and blends them linearly at the end; while effective locally, such stitching may limit global coherence. To improve longer-range structure, [17] adopts a two-stage choreography pipeline: a global diffusion model enforces sequence-level coherence, and a local diffusion model refines fine-grained movement quality. Despite their progress, 3D pipelines depend on costly paired 3D captures and require additional control to translate motion into person-specific, camera-aware videos. In parallel, 2D *in-the-wild* directions and end-to-end music→pose→video systems (e.g., [4]) commonly model raw 2D coordinates—often with autoregressive pre-

dictors. Our work focuses on the first stage, *music*→2D *pose*, within a diffusion framework, and studies how pose representation and temporal indexing affect alignment and temporal quality.

2D Pose Representations. Mainstream 2D human pose estimation (HPE) representations fall into three families. 2D raw representation methods directly predict continuous (x, y) coordinates without a grid [14, 32, 33], offering a lightweight alternative but historically trailing heatmaps in accuracy and stability. A large body of work adopts 2D Gaussian heatmaps for each joint, assigning per-pixel likelihoods on an $H \times W$ grid [2, 3, 23, 31, 36]. However, they incur significant memory/compute—especially for *sequences*, where generating T frames requires $O(T \times K \times H \times W)$ outputs for K joints. A third line discretizes coordinates into bins and uses one-hot [18] (or softened) vectors as targets, which have been shown to often outperform raw coordinate regression. Compared with full 2D heatmaps, per-axis one-hot encodings (for x and y) reduce the output dimensionality from $O(H \times W)$ to $O(W + H)$ per joint, which is attractive for long sequences ($O(T \times K \times (W + H))$) while retaining classification-style supervision that stabilizes training. In our setting, we adopt the one-hot pose representation for its balance between computational efficiency and generation stability.

3. Methods

Task Formulation. Given a 2D reference pose x_{ref} and a music clip of length t seconds, we aim to learn a model that generates a sequence of 2D dance poses $\hat{x}_{1:T}$ that are temporally coherent and rhythm-aligned with the music. Let the target frame rate be r (fps), so the sequence length is $T = r t$. A single-frame 2D pose is $x \in \mathbb{R}^{K \times 3}$, the k -th keypoint is (x_k, y_k, s_k) , where (x_k, y_k) are coordinates and $s_k \in [0, 1]$ is a detector confidence (typically lower under occlusion).

The reason for introducing a 2D reference pose as input is as follows. In downstream 2D pose-driven human image animation systems, videos are typically driven from a single reference image. This reference image is used to maintain the subject’s appearance, as well as the on-screen scale and background. Therefore, in our task formulation, we explicitly include a 2D pose *reference* to preserve the subject’s body proportions and on-screen scale, ensuring that the generated pose sequence is geometrically compatible with the input human image.

Overall Pipeline. Figure 1 outlines the pipeline. We first convert each pose frame into a one-hot representation. Stacking a sequence of such encodings across time yields a multi-channel, image-like tensor. We group chan-

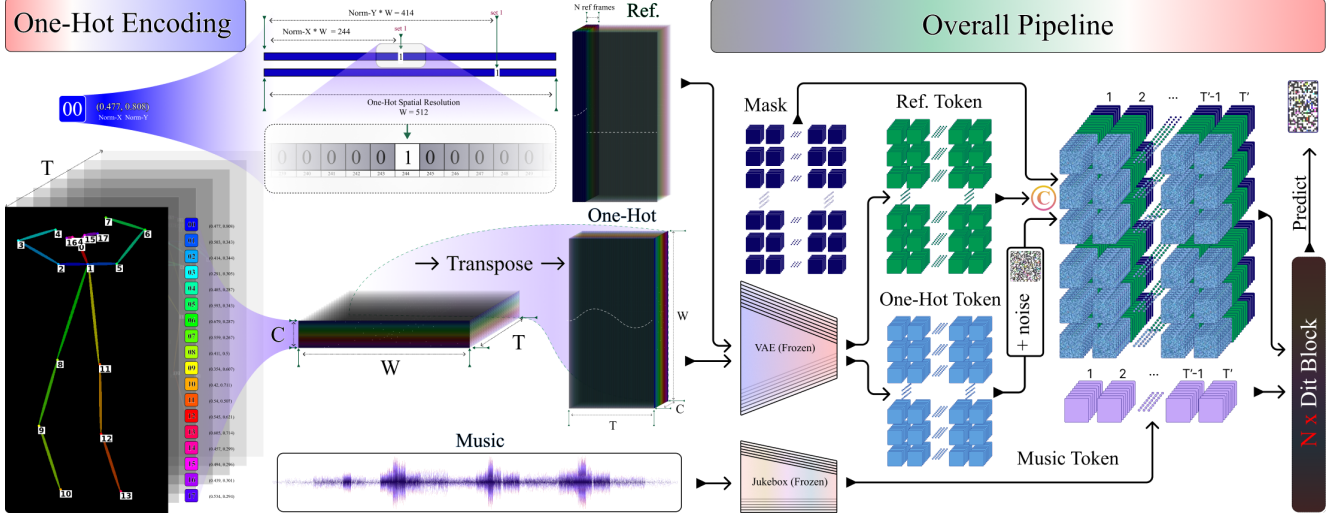


Figure 1. Left: Illustration of One-Hot encoding of 2D poses. Right: Overall Pipeline.

nels in triples and pass each triplet through a pretrained image VAE [28] to obtain a compressed latent representation Z . In parallel, the music is encoded into a token sequence using a pretrained music encoder JukeBox [6] whose hop size is chosen so that the token length matches the temporal length of Z . We assign positional indices so that the pose latent at column j and the j -th music token share the same time index. A diffusion-Transformer (DiT) [25] backbone receives noisy latents together with reference latents and a binary mask, predicts the noise, and iteratively denoises to produce \hat{Z} . Finally, a VAE decoder maps \hat{Z} back to \hat{X} , which is converted into the 2D pose sequence via arg max. Details are given in the following paragraphs.

One-Hot Pose Representation. Let $x \in \mathbb{R}^{K \times 3}$ denote the raw representation of a single-frame 2D pose, where the k -th keypoint is specified by its coordinate values $(x_k, y_k) \in [0, 1]^2$ (normalized image coordinates) and a confidence score $s_k \in [0, 1]$.

The one-hot pose representation encodes each coordinate value of each keypoint as a sparse vector. Take x_k as an example: we create a vector $H^{(k,x)} \in \mathbb{R}^W$ that is zero everywhere except at a single ‘hot’ index,

$$i_x = \lfloor W \times x_k \rfloor,$$

where W denotes the spatial resolution of the one-hot representation. The value at index i_x is set to the confidence score of that keypoint, i.e.,

$$H^{(k,x)}[i_x] = s_k.$$

Similarly, the y coordinate is encoded as another sparse vector $H^{(k,y)} \in \mathbb{R}^W$, where $H^{(k,y)}[i_y] = s_k$ and $i_y = \lfloor W \times$

$y_k \rfloor$. Stacking the sparse vectors of both x and y coordinates for all K keypoints yields $X \in \mathbb{R}^{C \times W}$ with $C = 2K$. Stacking T frames over time gives $X_{1:T} \in \mathbb{R}^{C \times W \times T}$.

Given the one-hot representation $X_{1:T} \in \mathbb{R}^{C \times W \times T}$, we can invert it to the raw coordinates by taking the indices of maximal entries. Let $c_x(k), c_y(k) \in \{0, \dots, C-1\}$ denote the channel indices of the x - and y -coordinates of the k -th keypoint in $X_{1:T}$, respectively. At the time- t , the sparse vectors are $X_{k,x,t} := X_{1:T}[c_x(k), :, t] \in \mathbb{R}^W$ and $X_{k,y,t} := X_{1:T}[c_y(k), :, t] \in \mathbb{R}^W$. Then the coordinates and the confidence score at time t are

$$x_{k,t} = \frac{1}{W} \left(\arg \max_{0 \leq d < W} X_{k,x,t}[d] \right). \quad (1)$$

$$y_{k,t} = \frac{1}{W} \left(\arg \max_{0 \leq d < W} X_{k,y,t}[d] \right). \quad (2)$$

$$s_{k,t} = \min \left\{ \max_{0 \leq d < W} X_{k,x,t}[d], \max_{0 \leq d < W} X_{k,y,t}[d] \right\}. \quad (3)$$

Using \min in Equation 3 yields a conservative score: only when both axes are strong is $s_{k,t}$ high.

Latent Encoding with a Pretrained VAE. Given $X_{1:T} \in \mathbb{R}^{C \times W \times T}$, note that for the same keypoint, the coordinate values evolve over time and thus form trajectory-like patterns along the temporal axis. Consequently, each channel in $X_{1:T}$ can be regarded as a $W \times T$ image whose pixel intensity is concentrated along curve-like traces over time axis. See left part of Figure 1 for an illustration. Following previous image-generation approaches that compress images into a compact latent space [28], we adopt an off-the-shelf image Variational AutoEncoder (VAE) to encode $X_{1:T}$ into a latent grid. Since the pretrained VAE is designed for 3-channel RGB inputs, we group the C channels

into $G = \lceil C/3 \rceil$ triplets (duplicating the last channel if necessary) and pass each triplet $\tilde{X}_g \in \mathbb{R}^{3 \times W \times T}$, $g = 1, \dots, G$, through the VAE encoder ϕ_e . The encoder produces 4 latent channels per triplet with an $8 \times$ downsampling along both W and T :

$$\tilde{Z}_g = \phi_e(\tilde{X}_g) \in \mathbb{R}^{4 \times W' \times T'}, \quad W' = \frac{W}{8}, \quad T' = \frac{T}{8}.$$

Concatenating all \tilde{Z}_g yields the final latent representation $Z \in \mathbb{R}^{(4G) \times W' \times T'}$. This grouping-and-compression strategy allows the same pretrained VAE to be reused across datasets with different numbers of keypoints K without re-training.

Music Tokens and Position-Index Synchronization. The music waveform is encoded by a pretrained music model ψ into a token sequence

$$A = \psi(\text{music}) \in \mathbb{R}^{T' \times d_a}.$$

Analogous to text tokens in text-to-image models, these music tokens can be paired with the pose latent grid (a 2D array of latent tokens), allowing us to reuse a DiT architecture without architectural modifications. However, common text-image setups (e.g., RoPE-based [30] encodings used in recent DiT models) assign 3D positional indices of the form $(0, w, t)$ to the image token at grid location (w, t) , while text token at position ℓ is assigned $(\ell, 0, 0)$ for $\ell = 0, \dots, L-1$. Such a design is suboptimal for music-to-pose because it does not explicitly couple the music and pose streams along time, which is crucial for rhythm alignment.

To promote rhythm alignment, we choose the music encoder's hop size so that the music token length matches the latent temporal length, i.e., $L = T'$. We then assign 3D indices that share the temporal coordinate t across modalities. For a pose token at position (w, t) and a music token at position t , their positional indices are

$$\text{pos}_{\text{pose}}(w, t) = (0, w, t), \quad \text{pos}_{\text{music}}(t) = (0, 0, t).$$

With $L=T'$ and shared temporal indices, the positional encoding (e.g., RoPE) makes pose token and music token phase-aligned along the time axis, increasing their positional affinity in cross attention. This design facilitates rhythm-aligned generation, as empirically shown in Section 4.2.

Reference-pose-based Conditioning Mechanism. We introduce a reference-pose-based conditioning mechanism with two objectives: (i) to preserve the body proportions and on-screen scale of a reference pose x_{ref} , and (ii) to improve temporal continuity when generating long sequences via a segment-and-stitch strategy. For (ii), we generate short

segments and stitch them; to reduce discontinuities at segment boundaries, we take the last N poses from the previous segment as references for the current segment so that the first N generated poses of the current segment are encouraged to match them.

To support both use cases within a single model, we construct a reference tensor

$$X_{\text{ref,repeat}} \in \mathbb{R}^{C \times W \times T}$$

by repeating the one-hot encoding of x_{ref} for T frames; this realizes the *shape-only* reference (body proportions without motion imitation). During training, we stochastically replace the first N frames of $X_{\text{ref,repeat}}$ with ground-truth poses with probability p , realizing *pose-aware* conditioning:

$$X_{\text{ref,repeat}}[:, :, 1:N] \leftarrow X_{\text{gt}}[:, :, 1:N].$$

The reference tensor is then encoded by the VAE to obtain

$$Z_{\text{ref}} \in \mathbb{R}^{(4G) \times W' \times T'}.$$

We further introduce a binary mask

$$M \in \{0, 1\}^{8 \times W' \times T'}$$

to mark which latent time locations correspond to replaced (pose-aware) reference frames, signaling the model to condition on the actual pose (rather than shape-only) at those times. More details about the mask construction are given in the supplementary material. Finally, we concatenate the noisy latents, Z_{ref} , and M along the channel dimension, and feed the result to the DiT backbone.

Training Objective and Inference. We adopt a DiT-style backbone f_{θ} operating on noisy latents with music conditioning and the positional indices described above. Let the forward noising process be

$$Z_{\tau} = \alpha_{\tau} Z + \sigma_{\tau} \varepsilon, \quad \varepsilon \sim \mathcal{N}(0, I), \quad \tau \sim \mathcal{U}\{1, \dots, S\},$$

where S is the total number of diffusion steps. The network predicts noise as

$$\hat{\varepsilon}_{\theta} = f_{\theta}([Z_{\tau} \parallel Z_{\text{ref}} \parallel M], A),$$

where \parallel denotes channel-wise concatenation and A are the music tokens. We train with the standard ε -prediction objective

$$\mathcal{L} = \mathbb{E}_{Z, \tau, \varepsilon} [\|\varepsilon - \hat{\varepsilon}_{\theta}\|_2^2].$$

At inference, iterative denoising yields \hat{Z} , which the VAE decoder ϕ_d maps to $\hat{X} \in \mathbb{R}^{C \times W \times T}$. We then recover the coordinates by inverting the one-hot representation using Eqs. (1), (2), and (3).

4. Experiments

4.1. In-the-Wild Training and Leakage-Free Testing

Datasets (i) **In-the-Wild-train**: we collect $\sim 30K$ dance videos from the web. After filtering (see details in the supplementary material), we obtain ≈ 600 hours and $240k$ training segments. (ii) **Leakage-free test set for In-the-Wild**. Preventing train-test leakage by music-identity at web scale is non-trivial: manual, song-level de-duplication across train/test is costly, and similarity-based retrieval (e.g., audio fingerprinting or embedding search) is prone to both false negatives (covers, remixes, key/tempo changes, background noise) and false positives (shared motifs or background tracks). To rigorously avoid train-test leakage, we froze all training downloads by July 2025. We then curated the test set in a *song-first* manner: we enumerated songs released strictly after July 2025 (based on public release dates) and collected dance videos for those songs only. By design, these test songs are guaranteed to be absent from the training set. The final test set contains 38 music-video pairs.

Evaluation. Following prior music-to-dance works [4], we report three metrics in the *2D pose space*: **FID** (\downarrow) for realism, **DIV** (\uparrow) for motion diversity, and **BAS** (\uparrow) for beat alignment. All metrics are computed in *2D pose space* to reflect our task focus. The exact 2D pose-space computation of FID/DIV/BAS is detailed in the supplementary material. We additionally conduct user studies on an in-house crowdsourcing platform with 50 raters. For each pairwise comparison, raters are shown two videos rendered from the generated 2D pose sequences as skeleton animations, synchronized with the same conditioning music. Raters are instructed to select the dance that “which of the two you prefer overall,” considering responsiveness to musical structure (e.g., tempo and section changes, downbeat accents), beat alignment, motion plausibility, realism, and variety; ties are not allowed. We report the Win Rate (WR, %), i.e., the fraction of trials in which our result is preferred over the baseline, in the corresponding comparison tables. Besides pose-space metrics (FID/DIV/BAS), we also report video-level metrics to approximate end-task quality: we feed the predicted 2D poses into a fixed pose-to-video renderer (Wan-Animate [5]) with identical settings across methods and compute FVD [35] and FID-VID [1] on the generated videos (lower is better).

Implementation details. Unless otherwise noted, we use a one-hot resolution of $W=512$ and temporal crops of $T=256$ frames. Our DiT backbone is the recent open-source text-to-image model *Lumina* (2.6B parameters) [27]. The image VAE and the music encoder (JukeBox [6]) are frozen; the DiT is trained from scratch with AdamW optimi-

mizer [20]. Following practice in pose detection tasks [18], we also apply Gaussian smoothing to each one-hot vector H before feeding it into the VAE. We employ classifier-free guidance [9] by randomly dropping the music conditioning with probability 0.3 during training. All models are trained on $8 \times H100$ (80 GB) GPUs. We train for 48K steps on In-the-Wild and 28K steps on AIST++2D. For the reference mechanism, the replacement length is set to $N=16$ frames during training. For long-audio conditional generation, we adopt a segment-and-stitch strategy: we generate fixed-length segments of 256 frames with an overlap of 16 frames and stitch adjacent segments. Consistent with our reference-pose conditioning, the first segment uses a *shape-only* reference and each subsequent segment uses the last 16 poses of the previous segment as *pose-aware* references to mitigate boundary artifacts.

Quantitative and Qualitative Results. We train our method on the collected large-scale In-the-Wild dataset and evaluate generalization on the leakage-free test set. First, we compare our model trained on 2D in-the-wild poses with methods trained on 3D motion datasets. Because 3D and 2D results cannot be directly compared with standard metrics—even when we project 3D motion to 2D (3D \rightarrow 2D projections use 17 joints, whereas 2D uses 18)—we rely on human evaluation with skeleton renderings instead. Table 2 summarizes the training data scale and human preference on the leakage-free in-the-wild test set. See supplementary videos in *S0_2Dvs3D-#.mp4*. All previous methods are trained on only 3.6–7.7 hours of paired music–3D motion, reflecting the difficulty of collecting mocap-quality 3D dance. With such limited supervision, these 3D-trained models struggle to generalize to unseen in-the-wild songs and are consistently preferred less than our 2D in-the-wild model. For a more controlled comparison, we also train our own architecture on the same 3D datasets (using 3D \rightarrow 2D projected poses); this variant still underperforms the identical architecture trained on 2D in-the-wild data, highlighting that the data regime—not just model design—is crucial for robust generalization. The 2D setting removes the bottleneck of 3D capture: we can scale training to 600 hours of in-the-wild dance videos, two orders of magnitude more data than any 3D baseline. As a result, this larger and more stylistically diverse corpus (covering broader musical genres, tempi, and body proportions) is key to the strong cross-genre and cross-style generalization we observe on unseen songs.

Next, we compare with representative music-to-dance systems from two families: diffusion-based methods (EDGE [34], LodGE [17]) and an autoregressive method (Bailando [29]). Xdancer [4] is conceptually the closest, but its code was not publicly available by the submission deadline. For a fair comparison, EDGE, Bailando, and LodGE

Table 1. Comparison on the In-the-Wild *leakage-free* test set (all methods retrained on same dataset for a fair comparison). “Ours-hand” predicts hand keypoints alongside body pose. Best in **bold**, second-best underlined.

Method	FID (↓)	DIV (↑)	BAS (↑)	FVD (↓)	FID-VID (↓)	WR
Bailando	110.62	6.62	0.2358	1589.48	107.05	98.32%
EDGE	80.36	3.88	0.2270	986.45	81.62	96.11%
LodGE	99.25	8.34	0.2336	1649.98	124.27	99.11%
Ours	45.20	<u>7.54</u>	0.2524	682.90	46.80	—
Ours-hand	<u>67.42</u>	6.39	<u>0.2518</u>	<u>876.36</u>	<u>58.78</u>	—

Method	Dur. (h)	Data Regime	WR
FACT [15]	5.2	3D	99.37%
Bailando [29]	5.2	3D	98.84%
EDGE [34]	5.2	3D	97.53%
POPDG [22]	3.6	3D	97.47%
LodGE [17]	7.7	3D	98.95%
Ours	5.2	(3D→2D)	99.68%
Ours	600	2D	—

Table 2. Comparison of methods trained under different 3D/2D data regimes.

were retrained on the same dataset using their publicly available code and recommended hyperparameters. Only necessary modifications were made to adapt the models for 2D pose training. Detailed descriptions of these changes can be found in the supplementary material.

The quantitative results are shown in Table 1, our model attains the best realism and rhythm alignment in pose space (lowest FID, highest BAS) and the best video-level quality when the poses drive a fixed pose-to-video renderer (lowest FVD/FID-VID). Diversity (DIV) is second-best—slightly below LodGE. Human preferences align with these trends: WR exceeds 95% against every baseline, indicating an overwhelming perceptual advantage. Beyond the raw numbers, we believe the gains stem from our reformulation. By casting pose generation as token-conditioned multi-channel *image* synthesis, we directly exploit the modern DiT-based token-conditioned image generation framework, which handles high-variance in-the-wild data well.

Supplementary videos provide side-by-side comparisons. We consistently observe stronger beat adherence, richer motion variety, and higher visual appeal for our method than for the retrained baselines. For example, in *S1_tempo-shift.mp4* at $t=3$ s, the music undergoes an abrupt tempo and energy change; our sequence promptly shifts amplitude and cadence to match, whereas compet-

ing results fail to adapt to the musical change, often persisting in low-energy or overly uniform motions that ignore the abrupt rhythm shift. For covers of the *same* song at different tempi, our dances scale naturally with tempo—see *S2_tempo-scaling-fast.mp4* (fast version) and *S2_tempo-scaling-slow.mp4* (slow version), where the step rate and per-beat motion extent follow the audio tempo. To illustrate stochastic diversity, we generate multiple dances for the *same* song by sampling different noise seeds; the choreographies are distinct (step patterns, amplitudes, phrasing) yet remain rhythm-aligned, see *S3_diversity-seeds.mp4*. Interestingly, our model also reflects camera motion: apparent subject scale changes (due to zoom/push) are mirrored smoothly in the pose without breaking rhythm; see *S4_camera-motion.mp4*. All visualizations are generated on the leakage-free test set, with *no* post-processing, highlighting the model’s generalization. More video examples *S5_more-#.mp4* are included in the supplementary. Figure 2 visualizes the generated 2D pose sequences together with the final dance frames produced by the downstream pose-to-video model.

Proportion-Aligned Evaluation. The baselines were originally designed for 3D motion generation and do not support reference input; consequently, their generated 2D poses may exhibit random body proportions and on-screen scale. Because our method can preserve the target proportion via a reference pose, one might worry that proportion alone could favor our pose/video FID/FVD. This concern is mitigated by our human evaluation control: raters are instructed to ignore body proportions and on-screen scale and to judge only considering responsiveness to musical structure, beat alignment, motion plausibility, realism, variety, and overall appeal. Even under this instruction, our method wins with $WR \geq 95\%$ against every baseline, indicating that the improvements are not attributable to proportion alone. At the same time, *this does not imply that FID/FVD are unreasonable metrics*. In our deployment set-



Figure 2. Comparison of generated 2D pose sequences and their rendered dance frames.

Method	FID (↓)	DIV (↑)	BAS (↑)
Bailando	40.76	8.10	<u>0.2694</u>
EDGE	37.55	<u>7.22</u>	0.1769
LodGE	<u>33.91</u>	5.50	0.1626
Ours	29.31	8.39	0.2715

Table 3. Comparison on the proportion-aligned AIST++2D test set.

ting, predicted poses are used to drive a fixed pose-to-video renderer (Wan-Animate); preserving subject proportion and on-screen scale materially affects visual utility. Proportion-aware, scale-aware metrics appropriately reflect whether the generated pose sequence faithfully preserves the target proportion needed for downstream rendering.

To remove proportion and on-screen scale effects, we also report results on **AIST++2D**. Starting from the original AIST++ [15] (1,408 curated 3D dance sequences with paired music), we obtain 2D poses by projecting the 3D motions with the dataset-provided calibrated cameras and a *canonical* (fixed) SMPL [19] body shape. We follow the official train/test splits. This standardization yields a consistent body proportion and on-screen scale across train and test, effectively neutralizing metric sensitivity to proportion/scale. Our method still outperforms the baselines on AIST++2D (Table 3), showing that the gains extend beyond proportion control.

Training with hand poses. We further extend our model to jointly predict full-body and hand poses, encoding hand keypoints as one-hot representation the same way as body

Rep.	FID (↓)	DIV (↑)	BAS (↑)	WR
Raw 2D	41.35	3.15	0.2432	
One-Hot (ours)	29.31	8.39	0.2715	78.50%

Table 4. Ablation on pose representation.

joints. In practice, hands are challenging: they contain a dense set of 42 keypoints that are spatially close, and VAE downsampling can blur or alias nearby fingers.

To mitigate this, we apply a simple, geometry-preserving preprocessing during training: we isotropically *enlarge each hand region around the wrist* by a fixed scale factor before forming the one-hot representation, so that the fingers occupy a larger pixel footprint (a “big-hand” view) and are better separated after VAE compression. Concretely, we scale each hand by proportionally lengthening the distance between every hand keypoint and the hand root (wrist): each keypoint is moved outward along the wrist–keypoint ray by a fixed factor, while the wrist itself remains unchanged. After generation, we apply the exact inverse scaling to map the predicted hand poses back to their original size. This procedure is deterministic and requires no changes to the network or loss—only a lightweight coordinate transform.

As demonstrated in Table 1, under the same model capacity, the pose metrics (FID/DIV/BAS) for Ours-hand (combining body and hands) are slightly inferior to those for Ours (body-only). This discrepancy reflects the increased complexity of the task. Nonetheless, Ours-hand still outperforms the retrained baselines in pose-space metrics and remains competitive in video-level metrics (FVD and FID-VID) when utilizing the fixed pose-to-video pipeline.

We visualize both body and hands skeletons and the final videos rendered by Wan-Animate; see S6_hand-#.mp4. Overall, the hand-aware dance poses exhibit rhythmically coordinated hand motions that align with the body pose and music, demonstrating approximate bilateral symmetry. However, we observe some high-frequency jitter at hand points during fast motions. We attribute this to noisy hand training data; in-the-wild dance videos often exhibit motion blur and self-occlusion, leading to noisy hand annotations. Our “big-hand” scaling alleviates, but does not eliminate, these artifacts. Despite these issues, the sequences remain rhythm-aligned and achieve better video-level metrics (FVD/FID-VID) than the retrained baselines, consistent with user-study preferences.

4.2. Ablation Study

We ablate three key design choices under a controlled setting: (i) pose representation (raw 2D vs. one-hot), (ii) positional indexing, and (iii) the reference-pose conditioning mechanism. For fairness, all ablations use the same DiT

backbone, optimizer, training schedule, and data splits on AIST++2D. We conduct ablations on AIST++2D because it is a clean, calibrated benchmark. This controls for confounders that could obscure the effect of the design factor itself—for example, raw 2D may look jittery on noisy in the wild clips for reasons unrelated to the representation. The results are as follows.

Representation (raw 2D vs one-hot). To maximize architectural parity in this ablation, we feed raw 2D poses to the DiT backbone (originally designed for image generation) as a “thin image.” Specifically, we reshape the raw pose representation $x_{1:T} \in \mathbb{R}^{K \times 2 \times T}$ into $Z_{\text{raw}} \in \mathbb{R}^{C \times 1 \times T}$ with $C=2K$ channels. No VAE is applied: Z_{raw} is treated as a grid latent and fed to the *same* DiT backbone as the one-hot variant, with only a minimal adjustment to the number of input channels. All other components—positional indices, conditioning modules, optimizer, and schedule—remain unchanged.

As shown in Table 4, switching from raw coordinates to our image-like one-hot representation yields consistent gains: FID decreases by 12.04 (41.35→29.31), DIV increases by 5.24, and BAS rises by 0.0283. Human evaluation also favors the one-hot variant with a WR of 78.5%. Qualitatively (see supplementary videos S7_ablation-1.mp4), the raw-2D model exhibits noticeable jitter, whereas the one-hot variant produces smoother, more stable motion with better beat adherence. Taken together, the experimental results suggest that, under the generation task setting, one-hot representations are better suited for pose generation than raw coordinates. This observation aligns with prior reports that one-hot is also better than raw in pose detection tasks [18].

Position-Index Synchronization. As shown in Table 5, replacing a common text–image indexing choice that does *not* share a temporal coordinate across modalities (“w/o time-shared t ”; image $(0, w, t)$, text $(\ell, 0, 0)$) with our *time-shared* indexing (pose $(0, w, t)$, music $(0, 0, t)$ with $L=T'$) improves rhythm alignment and motion variety without hurting realism. BAS increases by 0.0346 (0.2369→0.2715; +14.6%), DIV rises by 3.92 ($\approx 1.9 \times$), while FID remains essentially unchanged (29.38→29.31, -0.07). Human evaluation likewise prefers the time-shared variant (WR=64.7%). In supplementary videos S7_ablation-2.mp4, we form a slow→fast concatenation (with sharp style/tempo shift at the splice) using two audio clips from the AIST test. Our model switches choreography at the splice, while w/o time-shared indexing persists in the slow style. These results indicate that synchronizing temporal indices across modalities provides a precise cross-modal binding signal, enabling immediate, localized adaptation at change points. By contrast, without syn-

Indexing	FID (↓)	DIV (↑)	BAS (↑)	WR
w/o time-shared	29.38	4.47	0.2369	64.70%
ours	29.31	8.39	0.2715	

Table 5. Ablation on positional indices (non-time-shared vs. time-shared).

Ref. Cond.	FID (↓)	DIV (↑)	BAS (↑)	WR
Removed	31.77	8.24	0.2033	
Ours	29.31	8.39	0.2715	74.10%

Table 6. Ablation on reference conditioning.

chronization, the indexing acts like static semantic guidance (e.g., text-semantic conditioning): it offers only a global prior and cannot supply temporally-accurate references to the conditioning input.

Reference conditioning. To isolate the effect of reference conditioning, we train an ablated model that removes the reference conditioning. For stitching long sequences, this ablated model uses an inpainting-style strategy used by EDGE [34] analogous to masked inpainting diffusion for images [21]. As shown in Table 6, our reference conditioning improves beat alignment and realism over the removed baseline (FID 31.77 → 29.31, BAS 0.2033 → 0.2715). Human evaluation likewise prefers our method (WR=74%). Qualitatively (supplementary video S7_ablation-3.mp4), removing reference conditioning leads to visible discontinuities at segment boundaries, whereas our approach produces smoother transitions. A similar observation has been found in image inpainting, where approaches like [21] tend to produce seam artifacts at mask boundaries.

5. Discussion

We framed the music-to-2D pose task as token-conditioned multi-channel image generation, introducing time-shared positional indexing and reference-pose conditioning. This approach demonstrated a strong preference expressed by human evaluators. A key limitation lies in the quality of hand poses: in-the-wild dance videos often exhibit motion blur and self-occlusion, leading to low-recall and noisy hand annotations. These issues can propagate to training and may result in finger swaps or jitter during testing, even with our ‘big-hand’ scaling trick. Future work could focus on reducing label noise through higher-frame-rate hand crops, more robust hand detectors, or a lightweight hand-refinement head. Additionally, extending the model to accommodate multi-person interactions—such as contact, mirroring, and formations—using collision and spacing priors represents an intriguing avenue for further research.

References

[1] Yogesh Balaji, Martin Renqiang Min, Bing Bai, Rama Chellappa, and Hans Peter Graf. Conditional gan with discriminative filter generation for text-to-video synthesis. In *IJCAI*, page 2, 2019. [1](#) [5](#)

[2] Zhe Cao, Gines Hidalgo, Tomas Simon, Shih-En Wei, and Yaser Sheikh. Openpose: Realtime multi-person 2d pose estimation using part affinity fields. *IEEE Transactions on Pattern Analysis and Machine Intelligence*, 43(1):172–186, 2019. [2](#)

[3] Yilun Chen, Zhicheng Wang, Yuxiang Peng, Zhiqiang Zhang, Gang Yu, and Jian Sun. Cascaded pyramid network for multi-person pose estimation. In *Proceedings of the IEEE conference on Computer Vision and Pattern Recognition*, pages 7103–7112, 2018. [2](#)

[4] Zeyuan Chen, Hongyi Xu, Guoxian Song, You Xie, Chenxu Zhang, Xin Chen, Chao Wang, Di Chang, and Linjie Luo. X-dancer: Expressive music to human dance video generation. 2025. [1](#), [2](#), [5](#)

[5] Gang Cheng, Xin Gao, Li Hu, Siqi Hu, Mingyang Huang, Chaonan Ji, Ju Li, Dechao Meng, Jinwei Qi, Penchong Qiao, et al. Wan-animate: Unified character animation and replacement with holistic replication. *arXiv preprint arXiv:2509.14055*, 2025. [1](#) [5](#)

[6] Prafulla Dhariwal, Heewoo Jun, Christine Payne, Jong Wook Kim, Alec Radford, and Ilya Sutskever. Jukebox: A generative model for music. *arXiv preprint arXiv:2005.00341*, 2020. [3](#) [5](#)

[7] Patrick Esser, Sumith Kulal, Andreas Blattmann, Rahim Entezari, Jonas Müller, Harry Saini, Yam Levi, Dominik Lorenz, Axel Sauer, Frederic Boesel, et al. Scaling rectified flow transformers for high-resolution image synthesis. In *International conference on machine learning*, 2024. [1](#)

[8] Martin Heusel, Hubert Ramsauer, Thomas Unterthiner, Bernhard Nessler, and Sepp Hochreiter. Gans trained by a two time-scale update rule converge to a local nash equilibrium. In *Advances in Neural Information Processing Systems*, 2017. [1](#)

[9] Jonathan Ho and Tim Salimans. Classifier-free diffusion guidance. *arXiv preprint arXiv:2207.12598*, 2022. [5](#)

[10] Jonathan Ho, Ajay Jain, and Pieter Abbeel. Denoising diffusion probabilistic models. *Advances in neural information processing systems*, 33:6840–6851, 2020. [2](#)

[11] Li Hu. Animate anyone: Consistent and controllable image-to-video synthesis for character animation. In *Proceedings of the IEEE/CVF Conference on Computer Vision and Pattern Recognition*, pages 8153–8163, 2024. [1](#)

[12] Yuhang Huang, Junjie Zhang, Shuyan Liu, Qian Bao, Dan Zeng, Zheneng Chen, and Wu Liu. Genre-conditioned long-term 3d dance generation driven by music. In *ICASSP 2022–IEEE International Conference on Acoustics, Speech and Signal Processing (ICASSP)*, pages 4858–4862. IEEE, 2022. [1](#) [2](#)

[13] Buyu Li, Yongchi Zhao, Zhelun Shi, and Lu Sheng. Danceformer: Music conditioned 3d dance generation with parametric motion transformer. In *Proceedings of the AAAI Conference on Artificial Intelligence*, pages 1272–1279, 2022. [1](#), [2](#)

[14] Jiefeng Li, Siyuan Bian, Ailing Zeng, Can Wang, Bo Pang, Wentao Liu, and Cewu Lu. Human pose regression with residual log-likelihood estimation. In *Proceedings of the IEEE/CVF international conference on computer vision*, pages 11025–11034, 2021. [2](#)

[15] Ruilong Li, Shan Yang, David A Ross, and Angjoo Kanazawa. Ai choreographer: Music conditioned 3d dance generation with aist++. In *Proceedings of the IEEE/CVF International Conference on Computer Cision*, pages 13401–13412, 2021. [1](#), [2](#), [6](#), [7](#)

[16] Ronghui Li, Junfan Zhao, Yachao Zhang, Mingyang Su, Zeping Ren, Han Zhang, Yansong Tang, and Xiu Li. Finedance: A fine-grained choreography dataset for 3d full body dance generation. In *Proceedings of the IEEE/CVF International Conference on Computer Vision*, pages 10234–10243, 2023.

[17] Ronghui Li, YuXiang Zhang, Yachao Zhang, Hongwen Zhang, Jie Guo, Yan Zhang, Yebin Liu, and Xiu Li. Lodge: A coarse to fine diffusion network for long dance generation guided by the characteristic dance primitives. In *Proceedings of the IEEE/CVF Conference on Computer Vision and Pattern Recognition*, pages 1524–1534, 2024. [1](#), [2](#), [5](#), [6](#)

[18] Yanjie Li, Sen Yang, Peidong Liu, Shoukui Zhang, Yunxiao Wang, Zhicheng Wang, Wankou Yang, and Shu-Tao Xia. Simec: A simple coordinate classification perspective for human pose estimation. In *European Conference on Computer Vision*, pages 89–106. Springer, 2022. [2](#), [5](#), [8](#)

[19] Matthew Loper, Naureen Mahmood, Javier Romero, Gerard Pons-Moll, and Michael J. Black. SMPL: A skinned multi-person linear model. *ACM Trans. Graphics (Proc. SIGGRAPH Asia)*, 34(6):248:1–248:16, 2015. [7](#)

[20] Ilya Loshchilov and Frank Hutter. Decoupled weight decay regularization. *arXiv preprint arXiv:1711.05101*, 2017. [5](#)

[21] Andreas Lugmayr, Martin Danelljan, Andres Romero, Fisher Yu, Radu Timofte, and Luc Van Gool. Repaint: Inpainting using denoising diffusion probabilistic models. In *Proceedings of the IEEE/CVF conference on computer vision and pattern recognition*, pages 11461–11471, 2022. [8](#)

[22] Zhenye Luo, Min Ren, Xuecai Hu, Yongzhen Huang, and Li Yao. Popdg: Popular 3d dance generation with popdanceset. In *Proceedings of the IEEE/CVF Conference on Computer Vision and Pattern Recognition*, pages 26984–26993, 2024. [1](#), [2](#), [6](#)

[23] Alejandro Newell, Kaiyu Yang, and Jia Deng. Stacked hourglass networks for human pose estimation. In *European conference on computer vision*, pages 483–499. Springer, 2016. [2](#)

[24] Kensuke Onuma, Christos Faloutsos, and Jessica K. Hodgins. Fmdistance: A fast and effective distance function for motion capture data. In *Eurographics*, 2008. [1](#)

[25] William Peebles and Saining Xie. Scalable diffusion models with transformers. In *Proceedings of the IEEE/CVF international conference on computer vision*, pages 4195–4205, 2023. [1](#), [3](#)

[26] Qiaosong Qi, Le Zhuo, Aixi Zhang, Yue Liao, Fei Fang, Si Liu, and Shuicheng Yan. Diffdance: Cascaded human motion diffusion model for dance generation. In *Proceedings of the 31st ACM International Conference on Multimedia*, pages 1374–1382, 2023. [1](#), [2](#)

[27] Qi Qin, Le Zhuo, Yi Xin, Ruoyi Du, Zhen Li, Bin Fu, Yiting Lu, Xinyue Li, Dongyang Liu, Xiangyang Zhu, Will Beddow, Erwann Millon, Victor Perez, Wenhui Wang, Yu Qiao, Bo Zhang, Xiaohong Liu, Hongsheng Li, Chang Xu, and Peng Gao. Lumina-image 2.0: A unified and efficient image generative framework. In *Proceedings of the IEEE/CVF International Conference on Computer Vision (ICCV)*, pages 20031–20042, 2025. [1](#), [5](#)

[28] Robin Rombach, Andreas Blattmann, Dominik Lorenz, Patrick Esser, and Björn Ommer. High-resolution image synthesis with latent diffusion models. In *Proceedings of the IEEE/CVF conference on computer vision and pattern recognition*, pages 10684–10695, 2022. [3](#)

[29] Li Siyao, Weijiang Yu, Tianpei Gu, Chunze Lin, Quan Wang, Chen Qian, Chen Change Loy, and Ziwei Liu. Bailando: 3d dance generation by actor-critic gpt with choreographic memory. In *Proceedings of the IEEE/CVF Conference on Computer Vision and Pattern Recognition*, pages 11050–11059, 2022. [1](#), [2](#), [5](#), [6](#)

[30] Jianlin Su, Murtadha Ahmed, Yu Lu, Shengfeng Pan, Wen Bo, and Yunfeng Liu. Roformer: Enhanced transformer with rotary position embedding. *Neurocomputing*, 568:127063, 2024. [4](#)

[31] Ke Sun, Bin Xiao, Dong Liu, and Jingdong Wang. Deep high-resolution representation learning for human pose estimation. In *Proceedings of the IEEE/CVF conference on computer vision and pattern recognition*, pages 5693–5703, 2019. [2](#)

[32] Xiao Sun, Jiaxiang Shang, Shuang Liang, and Yichen Wei. Compositional human pose regression. In *Proceedings of the IEEE international conference on computer vision*, pages 2602–2611, 2017. [2](#)

[33] Alexander Toshev and Christian Szegedy. Deeppose: Human pose estimation via deep neural networks. In *Proceedings of the IEEE conference on computer vision and pattern recognition*, pages 1653–1660, 2014. [2](#)

[34] Jonathan Tseng, Rodrigo Castellon, and Karen Liu. Edge: Editable dance generation from music. In *Proceedings of the IEEE/CVF conference on computer vision and pattern recognition*, pages 448–458, 2023. [1](#), [2](#), [5](#), [6](#), [8](#)

[35] Thomas Unterthiner, Sjoerd Van Steenkiste, Karol Kurach, Raphael Marinier, Marcin Michalski, and Sylvain Gelly. Towards accurate generative models of video: A new metric & challenges. *arXiv preprint arXiv:1812.01717*, 2018. [5](#)

[36] Bin Xiao, Haiping Wu, and Yichen Wei. Simple baselines for human pose estimation and tracking. In *Proceedings of the European conference on computer vision (ECCV)*, pages 466–481, 2018. [2](#)

[37] Zhendong Yang, Ailing Zeng, Chun Yuan, and Yu Li. Effective whole-body pose estimation with two-stages distillation. In *Proceedings of the IEEE/CVF International Conference on Computer Vision*, pages 4210–4220, 2023. [1](#)

[38] Wenlin Zhuang, Congyi Wang, Jinxiang Chai, Yangang Wang, Ming Shao, and Siyu Xia. Music2dance: Dancenet for music-driven dance generation. *ACM Transactions on Multimedia Computing, Communications, and Applications (TOMM)*, 18(2):1–21, 2022. [1](#), [2](#)

Reframing Music-Driven 2D Dance Pose Generation as Multi-Channel Image Generation

Supplementary Material

6. Mask Construction Details (Reference Conditioning)

In our setup, the VAE uses a temporal stride of 8 (i.e., $T' = T/8$). Hence, one latent time column corresponds to 8 consecutive frames in the original sequence. We define a binary mask

$$M \in \{0, 1\}^{8 \times W' \times T'}$$

whose first dimension indexes the *frame-within-chunk* (phase). Each entry $M[\phi, x, t]$ specifies whether the latent at phase ϕ and latent time index t should be treated as *pose-aware* ($M = 1$) or *shape-only* ($M = 0$). Latents with $M = 1$ correspond to replaced reference frames where the model conditions on the actual 2D pose, whereas latents with $M = 0$ only provide shape-only context (e.g., shoulder width, limb lengths).

Given the number of replaced (pose-aware) reference frames $N \in \{0, 1, \dots, T\}$, let

$$q = \lfloor N/8 \rfloor, \quad r = N \bmod 8.$$

The mask M is then constructed as

(i) No replacement: $N = 0 \Rightarrow M = \mathbf{0}$ (all shape-only).

(ii) Full latent columns (pose-aware): $M[:, :, 0:q] = 1$.

(iii) Partial column (if $r > 0$, pose-aware phases):

$$M[0:r, :, q] = 1.$$

Intuitively, if N frames are replaced by pose-aware references, the first q latent time columns are fully pose-aware, while the remainder r indicates that, in the next column, only the first r phases (corresponding to the first r frames of that 8-frame chunk) are pose-aware and the remaining phases in that column remain shape-only. If $N \geq T$, we clamp q and r to valid ranges (i.e., not exceeding T' and 8, respectively). When $N = 0$, M is all zeros and the model conditions purely on shape-only references across the entire sequence.

7. In-the-Wild-Train Dataset Construction

We collect $\sim 30K$ in-the-wild dance videos from the web and apply the following preprocessing pipeline. First, we extract 2D poses for every frame using DW-Pose [37]. Then, we perform *shot-change filtering*: we compute inter-frame pose differences and treat frames whose difference exceeds a threshold as shot boundaries; only contiguous subsequences of at least 256 frames are kept. We also apply

a frame-rate sanity check, discarding videos whose native FPS is below 20 or above 60. After these filtering steps, we obtain ≈ 600 hours and $240k$ training segments.

8. 2D Pose-Space Metric Definitions

We adapt the commonly used FID, DIV, and BAS metrics to operate entirely in the 2D pose space. For FID, we compute the Fréchet Inception Distance [8] between the distribution of kinetic features [24] extracted from generated dances and that of the test-set dances. In the original formulation, these kinetic features are computed from 3D joint trajectories; in our setting, we recompute the same features from 2D keypoints so that FID is evaluated purely in 2D pose space. For DIV, consistent with FACT and Bailando, we measure motion diversity as the average pairwise distance between generated sequences in the kinetic-feature space. Again, the kinetic features are computed from 2D joint trajectories instead of 3D motions, yielding a diversity metric defined in 2D pose space. The Beat Align Score (BAS) is defined as the average temporal distance between each music beat and its closest dancing beat, where dancing beats are detected from the 2D pose sequence.

9. Baseline Adaptation Details

We retrain EDGE, LodGE, and Bailando on our 2D pose datasets using their publicly available code and recommended hyperparameters, making only the minimal changes described below. The original EDGE model predicts 3D motion parameters supervised by a 3D motion loss, a 3D joint-position loss, a 3D joint-velocity loss and a contact-consistency loss. In our 2D setting, we keep the joint-position and joint-velocity objectives but define them on 2D keypoints, replacing the 3D joint-position loss with a 2D keypoint-position loss and the 3D joint-velocity loss with a 2D keypoint-velocity loss. The 3D motion loss and the contact-consistency loss are removed because they cannot be computed from 2D keypoints. LodGE is modified in the same way. We retain the joint- and velocity-based losses and apply them to 2D keypoint coordinates, and we remove the 3D motion loss and the contact loss that explicitly depend on full 3D motion and contact patterns. For Bailando, which follows a multi-stage training pipeline, we modify two stages. In the VQ-VAE stage, we replace the original 3D keypoints with 2D keypoints as the reconstruction target while keeping the architecture unchanged. In the actor-critic learning stage, we omit this component entirely,

because its reward function depends on 3D joint angles that are unavailable in the 2D setting. Because none of the original three implementations provides a dedicated mechanism for handling invisible keypoints, we impute missing joints by temporal interpolation from neighboring frames, and discard sequences in which a large fraction of joints remains invisible.

10. Supplementary Videos

We provide additional qualitative results in the attached video folder accompanying this PDF. All videos are generated from either the leakage-free in-the-wild test set or the AIST++2D benchmark using the same settings as in the main paper, and are rendered either as skeleton animations or via the fixed pose-to-video renderer. Please watch the videos **with audio enabled**. The dance quality is best judged together with the music rhythm.

S0 2Dvs3D-#.mp4. Side-by-side comparisons between our 2D in-the-wild model and representative 3D-based music-to-dance methods under the data-regime setting in Table 2. Each clip shows skeleton renderings on the leakage-free test songs, illustrating the generalization gap between 3D-trained models and our 2D-trained generator.

S1 tempo-shift.mp4. An example with an abrupt tempo and energy change in the music. Our model promptly changes motion amplitude and cadence at the change point, whereas competing methods tend to continue low-energy or overly uniform motions, as discussed in Sec. 4.1.

S2 tempo-scaling-fast.mp4 and S2 tempo-scaling-slow.mp4. Covers of the same song at different tempi. These clips show that our generated dances naturally scale step rate and per-beat motion extent with the audio tempo.

S3 diversity-seeds.mp4. Multiple dances generated for the same song by sampling different diffusion noise seeds. The sequences demonstrate stochastic diversity in step patterns, amplitudes, and phrasing, while maintaining beat alignment.

S4 camera-motion.mp4. Examples with camera zoom/push. Apparent subject scale changes in the videos are mirrored smoothly in the generated pose without breaking rhythm.

S5 more-#.mp4. Additional qualitative results on the leakage-free test set, complementing the quantitative comparisons in Table 1.

S6 hand-#.mp4. Qualitative results for the hand-aware variant (Ours-hand). We visualize both full-body and hand skeletons together with the corresponding pose-to-video renders.

S7 ablation-1/2/3.mp4. Ablation videos corresponding to the studies in Sec. 4.2:

- **S7 ablation-1.mp4:** raw 2D coordinates vs. one-hot pose representation (Table 4), highlighting reduced jitter and improved stability for the one-hot variant.
- **S7 ablation-2.mp4:** without-time-shared vs. time-shared positional indexing (Table 5) on a slow→fast music concatenation; our indexing scheme switches choreography at the splice, whereas the baseline persists in the slow style.
- **S7 ablation-3.mp4:** with vs. without reference conditioning (Table 6) on long sequences, showing that removing reference conditioning leads to visible discontinuities at segment boundaries, while our model produces smoother transitions.